



ORIGINAL ARTICLE

Green sol–gel synthesis of hydroxyapatite nanoparticles using lemon extract as capping agent and investigation of its anticancer activity against human cancer cell lines (T98, and SHSY5)



Mahin Baladi ^a, Mahnaz Amiri ^{b,*}, Parisa Mohammadi ^b, Karrar Salih Mahdi ^c, Zahra Golshani ^d, Razieh Razavi ^e, Masoud Salavati-Niasari ^{a,*}

^a Institute of Nano Science and Nano Technology, University of Kashan, Kashan, P. O. Box. 87317-51167, Iran

^b Neuroscience Research Center, Institute of Neuropharmacology, Kerman University of Medical Science, 76175-113 Kerman, Iran

^c Medical Laboratories Techniques Department, Al-Mustaqbal University College, 51001 Hillah, Babylon, Iraq

^d Department of Chemistry, Shahid Bahonar University of Kerman, P.O. Box 76169-14111, Kerman, Iran

^e Department of Chemistry, Faculty of Science, University of Jiroft, Jiroft, Iran**Corresponding author.

Received 9 November 2022; accepted 29 January 2023

Available online 1 February 2023

KEYWORDS

Hydroxyapatite Nanostructures;
Cytotoxicity;
Green Synthesis;
Lemon extract;
T98 and SHSY5Y human cancer cell lines

Abstract Nanotechnology and biomedical sciences open the door to a wide range of biological research topics and medical applications at the molecular and cellular levels. Biosynthesis of nanoparticles has been proposed as a cost-effective and environmentally friendly alternative to chemical and physical methods. Plant-mediated synthesis of nanoparticles is a green chemistry approach that connects nanotechnology with plants. Novel methods of ideally synthesizing NPs are thus proposed that are formed at ambient temperatures, neutral pH, low costs and in an environmentally friendly fashion. The goal of the current study is to examine the cytotoxic activity of hydroxyapatite nanoparticles in various kinds of human cancer cells and potential mechanisms at play. Hydroxyapatite nanoparticles were created by the sol–gel method using lemon extract as a capping and reducing agent to achieve environmentally friendly synthesis. The synthesized nanoparticles were characterized by XRD, SEM, FTIR, TGA, VSM and HRTEM. They were tested for cytotoxicity against T98 and SH-SY5Y, two human cancer cell lines. The synthesized nanostructures significantly caused in vitro cell death in cancer cells. The results confirmed that synthesized nanoparticles significantly decreased the percentage of cells that survived. Nevertheless, it is essential to perform more investigations to find out the exact mechanisms involved. Binding energy

* Corresponding author.

Peer review under responsibility of King Saud University.



of Hydroxyapatite- SH-SY5Y complex and Hydroxyapatite- T98 complex calculated by molecular docking. However, it is essential to perform more investigations to find the underlying mechanisms.

© 2023 The Author(s). Published by Elsevier B.V. on behalf of King Saud University. This is an open access article under the CC BY-NC-ND license (<http://creativecommons.org/licenses/by-nc-nd/4.0/>).

1. Introduction

Cancer continues to pose a challenge to clinics because of its complexity and variety, despite its reputation as one of the deadliest diseases (Torre et al., 2012). The primary therapeutic strategy for cancer treatment at the moment is surgical resection followed by chemotherapy (Miller et al., 2016), but in many situations, the tumors are hard to remove all at once, and clinical chemotherapy has serious side effects, poor therapeutic efficacy, and poor cellular uptake (Chan et al., 2017). With the development of nanomaterials, chemotherapy has become more practical and effective (Xu et al., 2016).

Nowadays, inorganic material is one of the most popular choices for multifunctional drug delivery systems since it has undergone a lot of study recently, and has produced some impressive outcomes (Chen et al., 2015). Silica nanoparticles (Zhou et al., 2021), gold nanoparticles (Huang et al., 2021), and carbon-based compounds (Liu et al., 2018) are a few sample inorganic materials that have attracted a lot of attention, and have been the subject of extensive research. One of the most significant components of bones and teeth, hydroxyapatite, is an ideal substance for drug delivery due to its suitable biodegradability, strong bioactivity, and high biocompatibility (Sang et al., 2019). Additionally, hydroxyapatite is frequently employed for bone repair, tooth repair, and tissue engineering since it has been shown to have a significant impact on tissue healing (Wahl and Czernuszka, 2006).

Early in the 1970s, a bone marrow biopsy taken from a neuroblastoma patient with sympathetic adrenergic ganglionic origin led to the creation of the SH-SY5Y cell line. It is an SK-N-SH cell subline that has been cloned three times (Kovalevich and Langford, 2013). Since the early 1980s, this cell line has been frequently employed as a model of neurons since it possesses many functional, and biochemical characteristics of neurons. There are three distinct phenotypes of cells in the SK-N-SH cell line: intermediary (I type), Schwannian (S type), and neuronal (N type). A neuroblast-like cell line called SH-SY5Y is rather homogenous (N type) (Mateus, 2015). This cell line expresses one or more neurofilament proteins, as well as the neuronal marker enzymes tyrosine and dopamine-hydroxylases, selective absorption of norepinephrine (NA), and opioid, muscarinic, and nerve growth factor receptors (Arbo et al., 2016).

According to the World Health Organization, T98 is a grade IV glioblastoma (GB), which is an extremely infiltrative, and aggressive brain tumor (Bellail et al., 2004; Louis et al., 2016). Clinically, the primary causes of tumor relapse following surgery are GB's rapid tumor growth, invasion of the surrounding brain parenchyma, and inter-, and intra-tumoral heterogeneity (Claes et al., 2007). The most prevalent and dangerous form of tumor in adults' central nervous systems (CNS) is glioblastoma. Due to the recurrence of the disease, surgery is paired with chemo- and radiation for the treatment of glioblastoma (Ellor et al., 2014). But, the failure of the treatment is due to the tumor cells' resistance to chemotherapeutic medications (Messaoudi et al., 2015). The tumor necrosis factor-related apoptosis-inducing ligand (TRAIL), a member of the tumor necrosis factor (TNF) gene superfamily, interacts with the death receptors DR4, and DR5 to induce apoptosis in cancer cells (Zhao et al., 2017; Yuan et al., 2018). TRAIL is a popular chemotherapeutic medication because of its capacity to preferentially excite cancer cells while sparing healthy ones (Azijli et al., 2013). The greatest barriers to the therapeutic use of TRAIL, however, are its ineffective delivery, low solubility, short half-life, and resistance through a number of mechanisms in cancer cells (Wang, 2008). Glioma stem cells are resistant to TRAIL's ability to cause apoptosis, according to

research by Qi et al (Qi et al., 2011). As a result, for better clinical applications, new TRAIL sensitizing drugs are needed to increase TRAIL's apoptotic action. The development of novel nanomaterials (NMs) for use in biomedical applications has been made possible by breakthroughs in nanotechnology. Along with shape, size, and surface chemistry, NMs exhibit a variety of characteristics that depend on the type of material they are made of. Their exceptional qualities might lead to new ways to enhance or create anti-cancer therapeutic methods (De Wild et al., 2003; Altunbek et al., 2018).

The hydroxylated calcium phosphate-based substance hydroxyapatite (HAP), which possesses non-mutagenicity, non-toxicity, high biocompatibility, moderate long-term resorbability, and osteoconductive characteristics, has long been known for these qualities (Xiong et al., 2016; Kundu et al., 2013). This substance has been widely employed for bone scaffolds (Venkatesan et al., 2012), scaffold-based medication delivery systems (Mondal and Pal, 2019; Tao et al., 2021), and even for eye implants (Laonapakul, 2015) as well as dye removal (Sodhani et al., 2022; Vinayagam et al., 2022). HAP micro-granules, and microspheres have also been mentioned in several research as an injectable bone filler for the delivery of strong, long-lasting antibiotics (Geuli et al., 2017). However, the disadvantages of this material come from its porous structure and poor mechanical properties (Milovac et al., 2014). The characteristics, and chemical formula of synthetic hydroxyapatite are known to be identical to those of the primary inorganic component of teeth and, bones (Szczęs et al., 2017). As a result, for a while now this mineral has been widely used as a biomaterial for dental, and orthopedic applications to replace or repair hard tissues as well as as a means of medication administration.

For the synthesis of HAP, a variety of methods have been used recently, including biomimetic deposition, multiple emulsion, hydrothermal, sol-gel, and electrodeposition (Nosrati et al., 2020; Bakan et al., 2013; Nosrati et al., 2020). The sol-gel process is favoured over other options because of its uniform molecular mixing, high product purity, low synthesis temperature, and capacity to produce nano-sized particles. The synthesis of HAP via the sol-gel technique often results in a fine-grain microstructure made up of a variety of crystalline, nano- to submicron-sized particles. According to reports, these crystals are particularly effective in enhancing the stability, and contact at the artificial/natural bone interface seen in in vitro, and in vivo conditions. The precise molar ratio of 1: 1.67 between P, and Ca in the finished product is necessary for the synthesis of HAP using the sol-gel technique. Additionally, several alternative phosphorus, and calcium precursors are employed in the literature-reported sol-gel procedures for the synthesis of HAP. Also, a number of variables, including the crystal size and shape, impurity levels, precursor reagents, synthesis process, concentration and mixing order of reagents, temperature, and pH, affect the bioactivity of Ca-P based materials. The application determines which synthesis technique should be used.

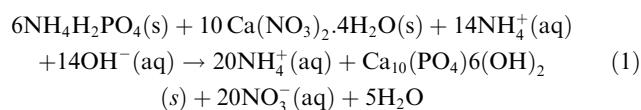
Chemical synthesis techniques result in the existence of some hazardous compounds that are adsorbed on surfaces, and might have negative consequences in medical applications. There are several advantages of eco-friendliness, and compatibility for pharmaceutical, and biological applications offered by the processes used to manufacture HAP particles utilizing ecologically mediated substances like plant extract. Furthermore, green template Synthesis (Parvathy et al., 2022; Subbaiya et al., 2017) seems to be superior to the chemical, and physical approaches since it is affordable, environmentally friendly, readily scaled up for large-scale synthesis, and does not require the use of harmful chemicals, high pressure, temperature, or energy. There are some papers that studied the anticancer effect of HA NPs on cancerous

cell lines. Ghate et al. synthesized the HAPnps by the leaf extract of *A. falcata* and the anti-cancerous effect of the synthesized HAPnps was studied on the viability of cancerous mammalian breast cell and lung cell lines (Ghate et al., 2022). In this study, a based sol-gel technique for the synthesis of pure nano-HAP was established utilizing $\text{NH}_4\text{H}_2\text{PO}_4$, and $\text{Ca}(\text{NO}_3)_2 \cdot 4\text{H}_2\text{O}$ as phosphorus (P), and calcium (Ca) precursors. As a result, the current study uses the green chelating agent as a template for the synthesis of HAP powders by employing plant extracts as chelating agents. This includes the extract of lemon. This work is the first to report on the green production of hydroxyapatite nanoparticles in the presence of lemon extract. The sol-gel auto combustion process was used to create the nanoparticles. The purity, size, and shape of the nanoparticles were examined. The antitumor activity of the created nanostructures was tested on cancer cell lines (T98 and SHSY5Y). Molecular docking has been done for calculating the binding energy and van der Waals as well as the electrostatic surface of Hydroxyapatite- SH-S5YS complex and Hydroxyapatite- T98 complex.

2. Materials and methods

2.1. Materials

Nano-HAP was created using a relatively straightforward procedure. The experimental process utilized to produce the nano-HAP is described in the flow chart provided in Scheme.1. $\text{NH}_4\text{H}_2\text{PO}_4$, and $\text{Ca}(\text{NO}_3)_2 \cdot 4\text{H}_2\text{O}$ were employed as the initial P, and Ca precursors in the synthesis. The solution's pH was adjusted with ethylenediamine (en). The following synthesis reaction was performed:

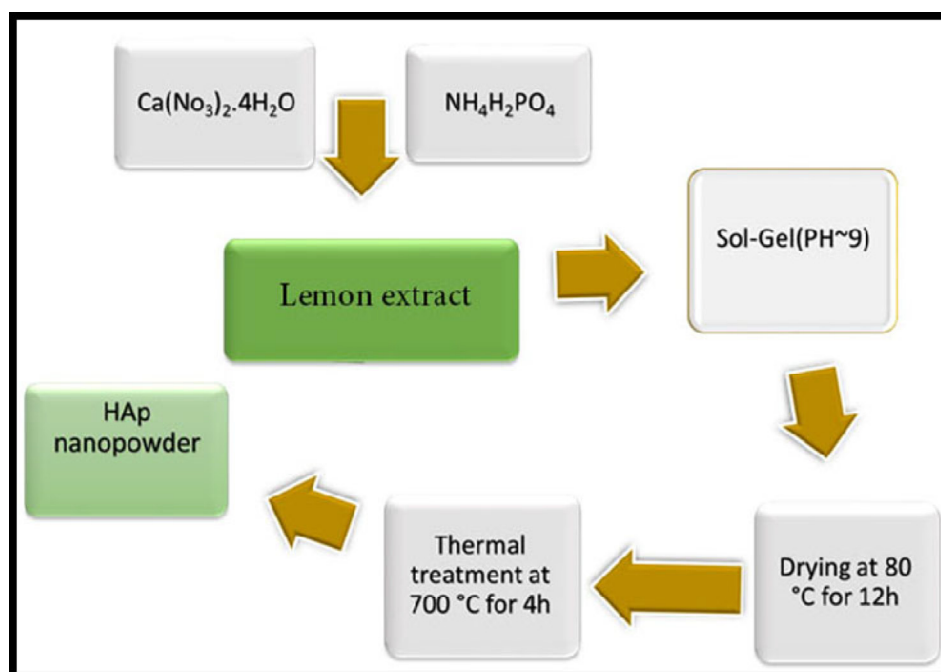


2.2. Preparation of extract

Lemons were pressed to extract juice which was later strained through a fine-pore nylon mesh. The juice obtained was centrifuged at 10,000 rpm for 10 min to remove any undesired impurities. Further experiments will be conducted using this juice.

2.3. Synthesis of HAP nanocrystals

Typically, a reaction between an ammonium hydrogen phosphate solution and a calcium-ligand solution produces HAP nanocrystals. Ca/P, and Ca/ligand had molar ratios of 1.67, and 1.0, respectively. In order to create hydroxyapatite NPs using the sol-gel method, first 0.57 g (1.0 M) of $\text{NH}_4\text{H}_2\text{PO}_4$, and 1.97 g (1.67 M) of $\text{Ca}(\text{NO}_3)_2 \cdot 4\text{H}_2\text{O}$ ($\text{Ca}/\text{P} = 1.67$) were first dissolved separately in a certain volume of distilled water. After 10 min of complete dissolution at room temperature on a magnetic stirrer, a natural reducing and capping agent (lemon extract) was slowly added. Lemon extract was used as a biological source of citric acid that acts both as a reducing agent to favor the hydrolysis of the precursor molecules and as a capping agent that hinders the surface chemical reactivity of the nanoparticles via the formation of strong coordination between citrate ions and the Hap ions so that the aggregation of the resulting nanoparticles could be reduced (Navaneethan et al., 2017). After that, ethylene diamine was added dropwise to the aforementioned solution to change the pH value to 9. The resultant mixture was heated for 30 min at 50 °C, then the temperature was raised to 120 °C until a viscous gel was obtained. This was then transferred to an oven for 12 h at 80 °C. Through calcination at 700 °C for 4 h, a white hydroxyapatite powder was obtained.



Scheme 1 The formation process of the hydroxyapatite NPs powders by sol-gel auto-combustion method using the lemon extract as combustion agent.

On a Shimadzu IR-460 spectrometer, KBr pellets' Fourier transform infrared (FT-IR) spectra were recorded between 400 and 4000 cm^{-1} . A diffractometer from the Philips Company was used to capture powder X-ray diffraction (XRD) patterns using X'Pert Pro monochromatized Cu $K\alpha$ radiation ($\lambda = 1.54 \text{ \AA}$). Scanning electron microscopy, also known as Field Emission SEM (FE-SEM) (Mira3 Tescan), is employed to evaluate the particle size of pure nano-HAP. Also, the sputter coating procedure involves covering the samples with an incredibly thin layer of gold prior to SEM examination. The Philips XL30 microscope was used to study the analysis of EDS (Energy Dispersive Spectrometry). Transient electron microscopy (TEM) and a HRTEM operating (HT-7700) were utilized to measure the particle size and morphology of nano-HAP samples. To prepare the grid for TEM examination, a tiny amount of material was first sonicated for 20 min to make it evenly disseminated in 20 mL of ethanol. Vibrating sample magnetometers (VSMs) were used to measure magnetic characteristics (Meghnatis, Daghigh Kavir Co.; Kashan Kavir; Iran). Using an automated gas adsorption analyzer, N2 adsorption/desorption analysis (BET) was carried out at 196 °C (Tristar 3000, Micromeritics).

2.4. Cell viability

MTT dye reduction, in which MTT was lowered by active mitochondria in live cells, was used to indirectly calculate the proportion of viable cells. The MTT test was carried out using the modified procedure described by Sladowski et al. (Sladowski et al., 1993). Briefly, in 96-well Iwaki plates, 2×10^2 cells were incubated for 2 h at 37 °C, and 5 % CO_2 with 1 mg/mL of MTT in DMEM. The decreased MTT formazan crystals were dissolved in 250 mL of DMSO after three rounds of washing with 0.2 M phosphate buffer saline (PBS) at pH 7.4. After that, an enzyme-linked immunosorbent assay (ELISA) reader (Pharmacia Biotech, Stockholm, Sweden) measured the optic density (OD) at 570 nm.

2.5. Statistical analysis

Software from the statistical package for social science (SPSS) version 16 was used for data analysis (IBM, Armonk, NY, USA). The information was shown as mean standard error of the mean (SEM). *T*-Student's test with a 95 % confidence level was used to assess the significance between the treatment and control groups. *P*-values of 0.05 or less were regarded as significant.

2.6. Molecular docking

We have applied the MOE software to calculate binding energy, van der Waals, and electrostatic map surfaces of Hydroxyapatite-SH-S5YS complex and Hydroxyapatite-T98 complex. For receptor preparation and preprocessing, T98 and SH-S5YS structures were downloaded from PDB bank data. Crystal Maker software was used to create the hydroxyapatite.

3. Results and discussion

3.1. X-ray analysis

Using a Cu $K\alpha$ X-ray diffractometer crystallinity, phase composition, and the purity of the HAP powders as produced were identified. The X-ray patterns of hexagonal hydroxyapatite nanoparticles made with lemon extract at various temperatures are shown in Fig. 1, and the XRD patterns of the nanoparticles produced at 700 °C for 4 h are shown in Fig. 2. Peaks associated with plates with (100), (111), (002), (211), (112), (300), (202), (222), and (213) which are in agreement with XRD results (JCPDS file no. 00-024-0033). The existence of sharp peaks can be attributed to the hexagonal phase hydroxyapatite with the space group of $P63/m$ and cell constants $a = b = 9.4240 \text{ \AA}$, and $c = 6.8790 \text{ \AA}$. Scherer equation $D = K\lambda / \beta \cos\theta$ (K is the required shape factor, λ is the wavelength of the X-ray source employed to XRD, θ is the Bragg angle, and β is line broadening at half the maximum intensity) was used to estimate the average size of the crystals in the sample (Salavati-Niasari et al., 2009). The sample's estimated domain

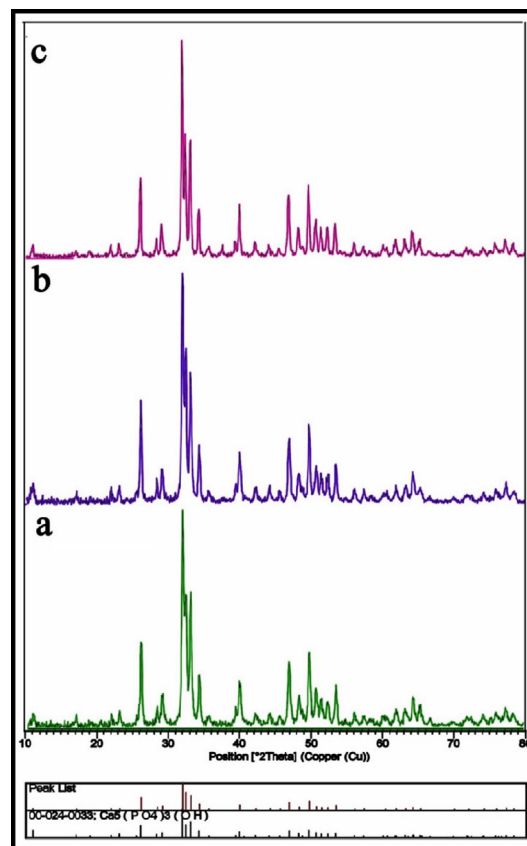


Fig. 1 XRD patterns of the HAP NPs provided in the presence of lemon extract at various calcination temperatures: (a) 600 °C, (b) 700 °C, and (c) 800 °C for 4 h.

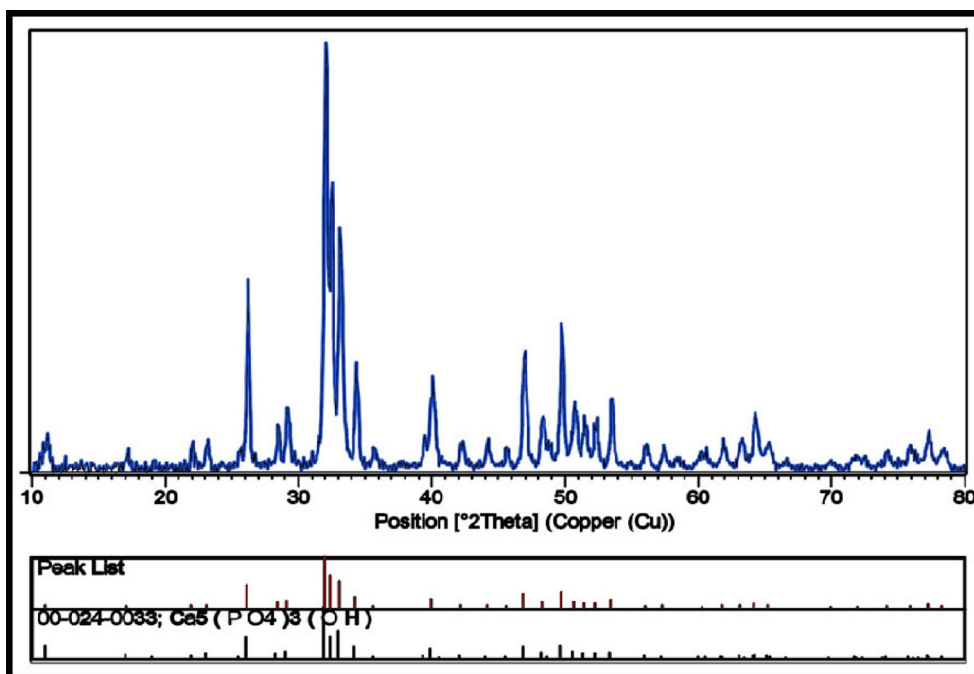


Fig. 2 XRD patterns of the HAP NPs provided at calcination temperatures 700 °C for 4 h.

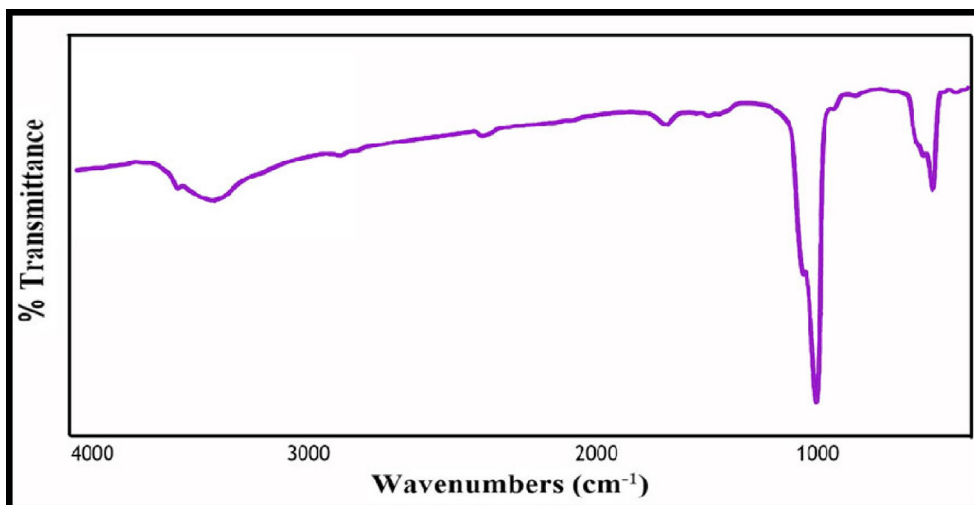


Fig. 3 The FTIR spectrum of hydroxyapatite NPs prepared in presence of lemon extract at 700 °C for 4 h.

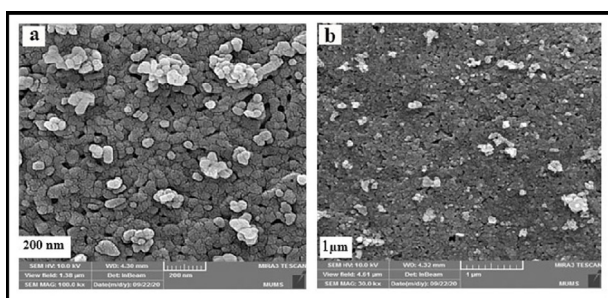


Fig. 4 SEM images of hydroxyapatite NPs prepared in presence of lemon extract at 700 °C for 4 h.

size is 27 nm. The separation of peaks is appropriate, which indicates that the crystal structure is single-phase and there are no impurities in the sample.

3.2. FTIR spectra analysis

The FT-IR spectra of the sample are shown in Fig. 3 along with the assignments of the observed vibrational frequencies of the nano-HAP produced using lemon extract. Without any trace of contaminants, all of the peaks seen in the FT-IR spectrum are attributable to the characteristic peaks of HAP. To explain them, the ν_1 phosphate mode, which is seen at 605 cm^{-1} , 568 cm^{-1} , and 1045 cm^{-1} , is ascribed to the triply

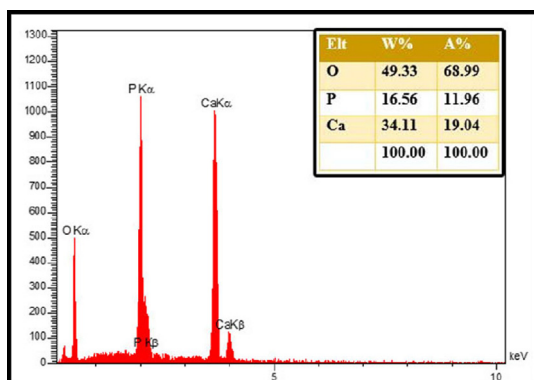


Fig. 5 EDS patterns of hydroxyapatite NPs prepared in presence of lemon extract at 700 °C for 4 h.

degenerate asymmetric P—O stretching peak, the phosphate group's ν_4 , ν_3 mode, and the triply degenerate asymmetric P—O stretching peak, respectively. The phosphate's ν_2 vibrational mode is observed at 472 cm⁻¹.

Additionally, at the peak locations of 3500 cm⁻¹, the vibration modes of hydroxyl bending and stretching are seen. The hydroxyl peak is regarded as the HAP confirmative peak. Lattice water adsorption was also discovered at 1633 cm⁻¹, and 3435 cm⁻¹ in the bending, and stretching modes. Additionally, the very sensitive FTIR data show no C—H stretching vibra-

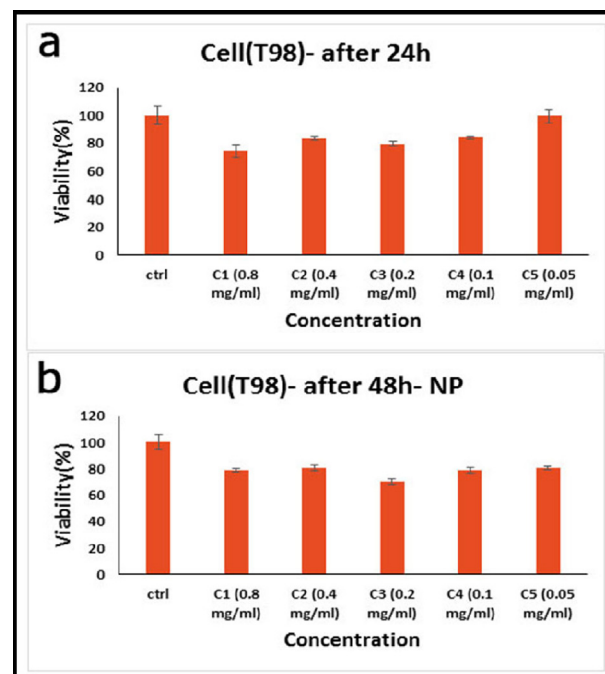


Fig. 8 In vitro cell viability assay, Cell viability of T98 cell lines incubated with hydroxyapatite NPs at different concentrations for (a) 24 h, and (b) 48 h (SD \pm 2 %).

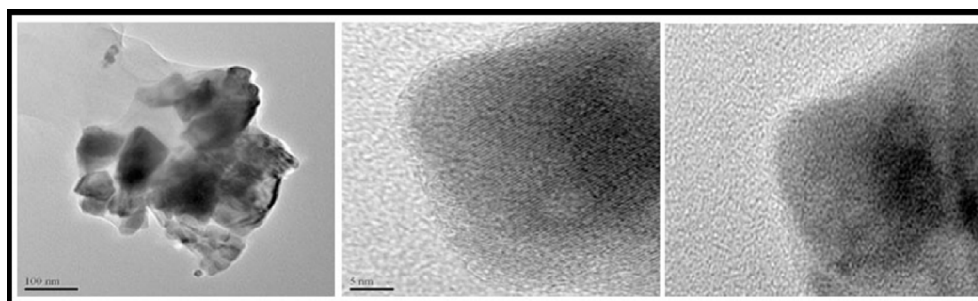


Fig. 6 TEM images of hydroxyapatite NPs prepared in presence of lemon extract at 700 °C for 4 h.

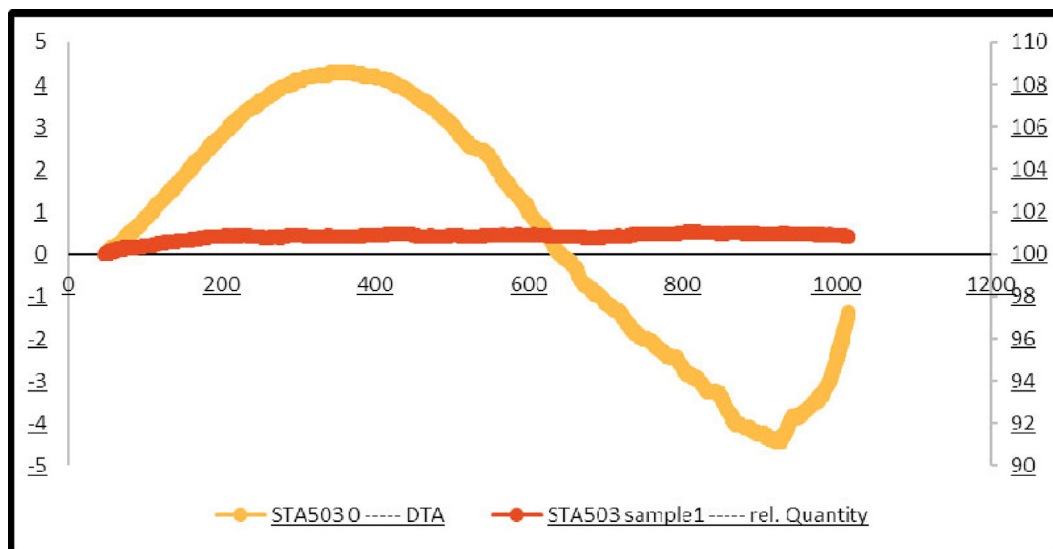


Fig. 7 TGA spectrum of hydroxyapatite NPs prepared in the presence of lemon extract, and calcined temperature of 700° C for 4 h.

tional peaks, indicating the purity of the HAP sample and the absence of any organic groups (Bakan et al., 2013).

3.3. Morphology and microstructure analysis using FE-SEM

In Fig. 4, the FE-SEM method was used to demonstrate the grain size and shape of the green synthetic hydroxyapatite nanoparticles in the presence of a natural extract. Images show the sample in particle form, and the particle structure appears to be almost regular. The particle size was calculated in the range of 25–35 nm. The elemental composition of nano-HAP is revealed by the EDX spectra of the produced powders before and after heat treatment, which are depicted in Fig. 5. Since no additional significant elements have been found, clear peaks for O, P, and Ca were obtained. This research determined the Ca/P ratio to be around 1.59, demonstrating the purity of HAP.

3.4. Morphology and microstructure analysis using HR-TEM

By using TEM analysis, the surface size, and morphology of the produced nanoparticles were also examined. In Fig. 6, Two magnifications of HR-TEM pictures of produced nanoparticles

are shown. As seen in Fig. 6. Particles between 30 and 40 nm in size that are substantially spherical are clumped together.

3.5. Thermogravimetric analysis (TGA/DTA)

TGA was performed in a nitrogen environment between 30 and 1200 °C on a dried sample that had been aged in the air for 48 h. Several thermal events are shown in Fig. 7. The loss of water that has been adsorbed in the substance is what causes the first one, which occurs at 130 °C. The loss of structural water causes the second one, which occurs at about 280 °C. Two molecules of calcium monohydrogen phosphate react at 450 °C to create pyrophosphate, and water in the third event. Since hydroxyapatite nanoparticles were created in their purest state, a steady mass loss compared to its dehydroxylation would be anticipated to begin at about 600 °C (Catauro et al., 2019).

3.6. Green synthesis hydroxyapatite NPs cytotoxicity studies

We compared the inhibitory effects of green synthesis hydroxyapatite NPs on the cell proliferation of cancer cells using MTT assay. Fig. 8 indicated in vitro cell viability assay, cell

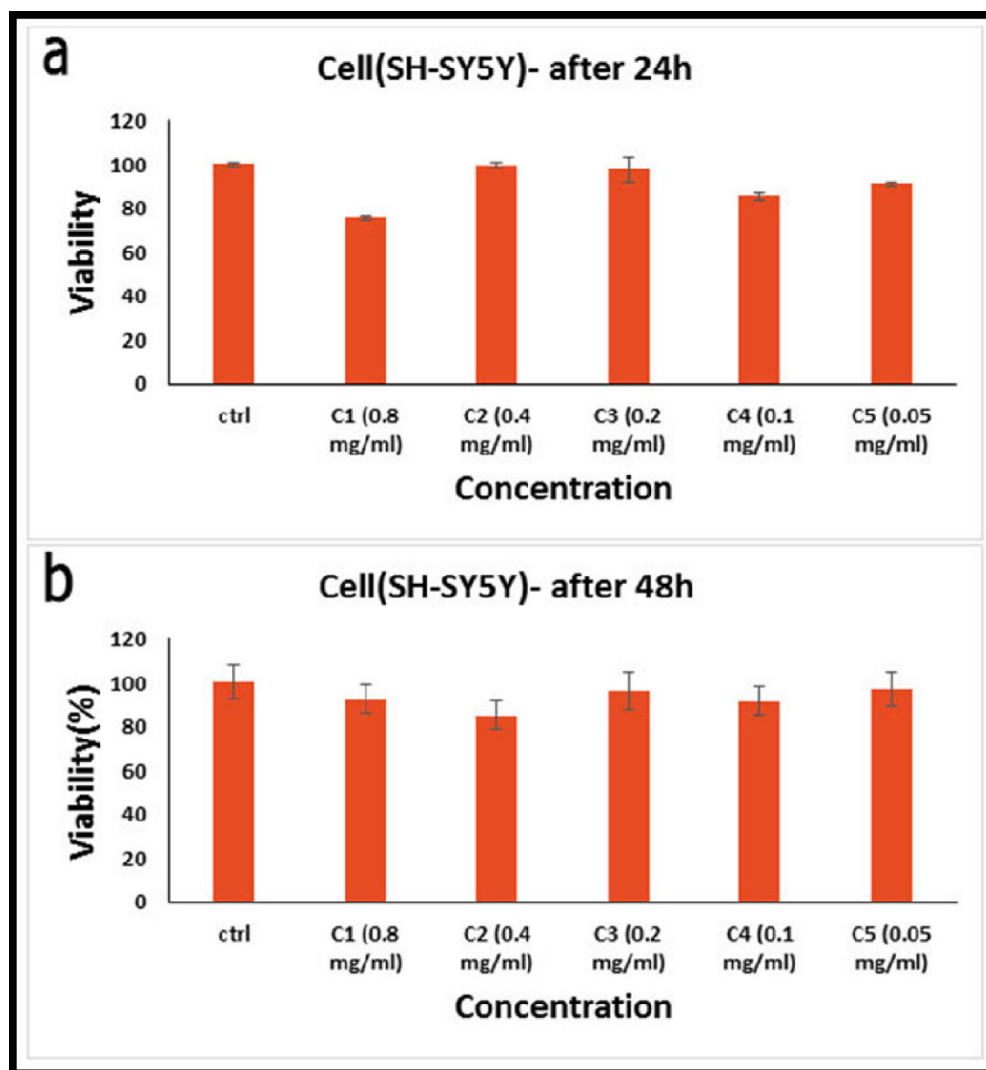


Fig. 9 In vitro cell viability assay, Cell viability of SH-SY5Y cell lines incubated with hydroxyapatite NPs at different concentrations for (a) 24 h, and (b) 48 h (SD ± 2 %).

viability of T98 cell lines incubated with green synthesized hydroxyapatite NPs at different concentrations for (a) 24 h, and (b) 48 h. Viability was noticeably decreased in cultivated cells when NPs were present at various doses, suggesting a dose-dependent effect. According to Fig. 8, the NPs demonstrated a strong indicator of cytotoxicity impact on cancerous cell lines. The fact that glioblastoma cells demonstrate rapid cell division, and a more rapid rate of metabolism, as well as better NPs internalization, may be the cause of the inhibitory effects of NPs on this tumour. This increased internalization results in a higher rate of cell death (Goudarzi et al., 2021). With the passage of time, the level of toxicity in different concentrations increases, but the level of toxicity in different doses becomes similar to each other. In total, all the NPs showed similar levels of toxicity to this cell at 24, and 48 h.

Fig. 9 reported the in vitro cell viability assay, cell viability of SH-SY5Y cell lines incubated with hydroxyapatite NPs at different concentrations for (a) 24 h, and (b) 48 h. In addition to the production of reactive oxygen species, the lower cellular ATP level, and decreased dehydrogenase activity cause damage to the mitochondrial respiratory chain, and other cellular components, leading to cell death, which is the cause of the decreased cell viability against NPs. Therefore, rather than causing a general disruption in cell membrane functions, phyto-genic NPs' cytotoxicity is reliant on the kind of cell that exhibits a unique intracellular mechanism for growth suppression. However, the only factors that determine an NP's cytotoxicity

are its interaction duration, surface chemistry, size, shape, and aggregation state (Amiri et al., 2018). Consequently, the toxicity level of all NPs was higher in glioblastoma cells than in neuroblastoma cells. The duration of treatment is another factor that affects nano-ability HAP's to inhibit cell proliferation. Fig. 10.

Additionally, it was claimed that HAP NPs encourage the production of p53 and its downstream genes in tumor cells, which results in apoptosis (programmed cell death) (Sun and Ding, 2009). According to Tang et al., HAP causes apoptosis and reduces cell growth in several cancer cells by activating caspase-3, and -9 (but not caspase-8) (hepatoma cells [HepG2], cervical adenocarcinoma epithelial cells [HeLa], and gastric cancer cells [MGC80-3]) (Tang et al., 2014). Also, the anticancer effects of HAP NPs were studied on human

Table 1 Stability energy of compounds.

Compound	ΔG (kcal /mol)
Hydroxyapatite	-2.086×10^3
T98	-1.079×10^4
SH-S5YS	-7.46×10^3
Hydroxyapatite- T98 complex	-1.53×10^4
Hydroxyapatite- SH-S5YS complex	-9.62×10^3

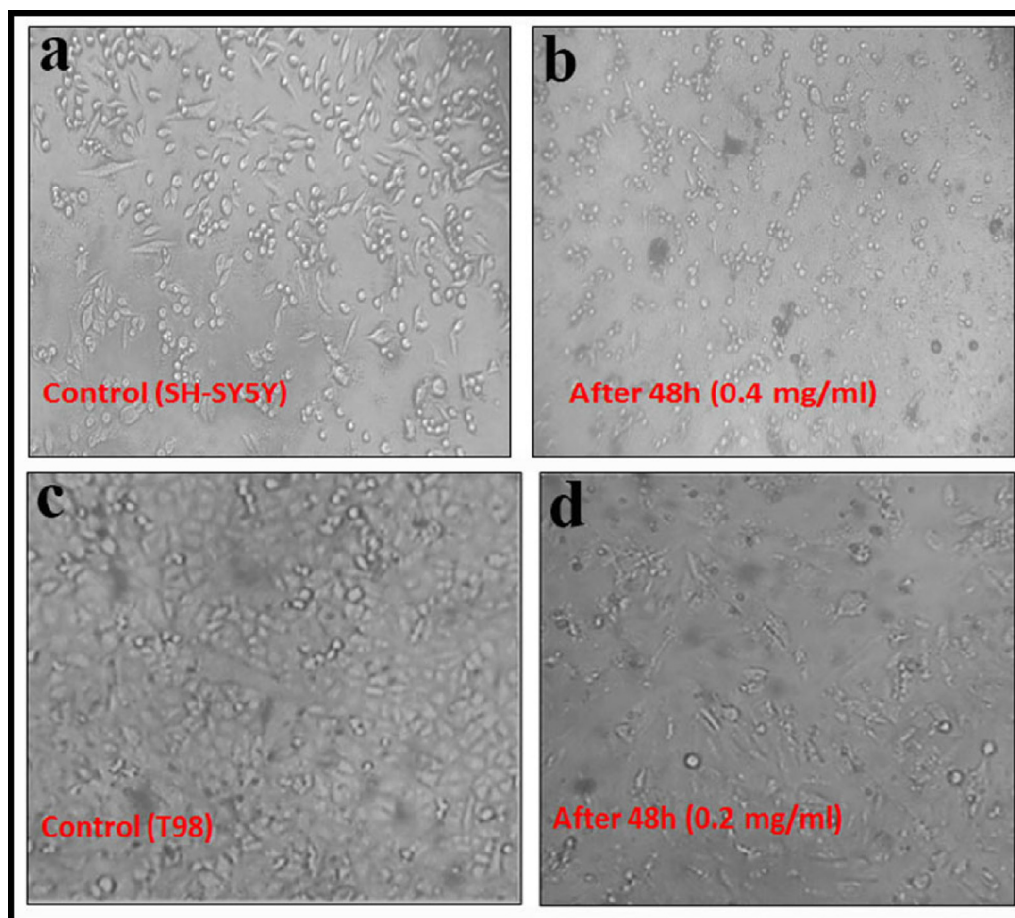


Fig. 10 The images of cell viability after 24 and 48 h; SH-SY5Y (a, b) and (c,d) T98.

glioma SHG44, and U251 cells both in vivo, and in vitro, in a different publication (Chu et al., 2012). 48 h after incubation, HAP NPs at concentrations of 120 mg/L, and 240 mg/L caused apoptosis. Further, the cellular tumor development capability was inhibited following the injection of HAP NPs in vivo in a rat model, and the associated adverse effects of the chemotherapy agent 1,3-bis(2-chloroethyl)-1-nitrosourea (BCNU) were greatly reduced if it was given along with HAP NPs. The anticancer effect of HAP NPs was ascribed to a decrease in the expression of Bcl-2, Ki-67, SATB1, and c-Met, protein, caspase-3, and SLC22A18.

Other experimental studies have shown that HAP NPs generate and contribute to the intracellular buildup of reactive oxygen species (ROS), which harm the DNA of cancer cells (Salavati-Niasari, 2006). High concentrations of HAP NPs can be absorbed by endocytosis in cancer cells in the endoplasmic reticulum, inhibiting protein synthesis by lowering the binding of mRNA to the ribosomes in cells, and stopping the cell cycle in the G0/G1 phase. It is worth noting that the addition of certain elements (such as Se) into the structure of nano-sized HAP may enhance its anticancer effects (Zhou et al., 2019). Despite the fact that a connection exists between HAP-NPs' physico-chemical characteristics, and their anticancer effects, generalizing this link is still a long way off. This is a result of the variety of factors involved, their interdependent synergy, and the variation in response between various cancer cell types.

3.7. Docking analysis

Binding energy; the amount of energy required to separate a particle from a system of particles or to disperse all the particles in the system. Binding energy is especially applicable to subatomic particles in atomic nuclei, to electrons attached to nuclei in atoms, and to atoms and ions bonded together in crystals. Binding energy of Hydroxyapatite with T98 and SH-S5YS Table 1 calculated by Amber10 force field. Data in

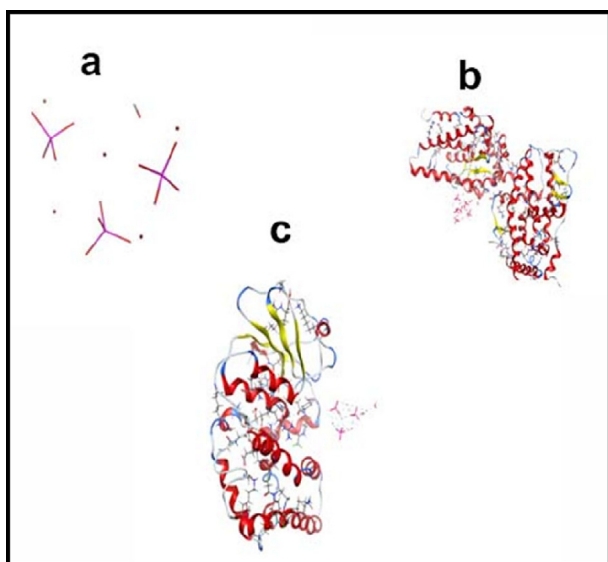


Fig. 11 Optimized structure of (a) hydroxyapatite, (b) Hydroxyapatite-T98 complex and (c) Hydroxyapatite-SH-S5YS complex.

Table 1 illustrate the stable structure of each receptor and confirm the strong binding between Hydroxyapatite and receptors. Fig. 11 presents the optimized structure of (a) hydroxyapatite, (b) hydroxyapatite-T98 complex and (c) hydroxyapatite-SH-S5YS complex. Van der Waals interactions are at the heart of chemical physics. EPS-mapped van der Waals surfaces (kcal/mol) using a color scale ranging from red (negative EPS) through white (neutral EPS) to blue (positive EPS). The blue regions indicate a vulnerable site for nucleophilic attack, and the red regions are sites for electrophilic attack. Fig. 12, which displays the electrostatic surface of Hydroxyapatite, confirms the repulsion site of this molecule. Figs. 13 and 14, show the van der Waals surface map of Hydroxyapatite, T98, SH-S5YS, hydroxyapatite-SH-S5YS complex and

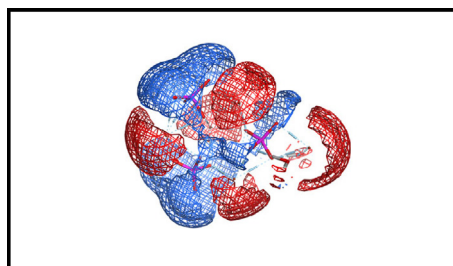


Fig. 12 Electrostatic map of hydroxyapatite nanoparticles.

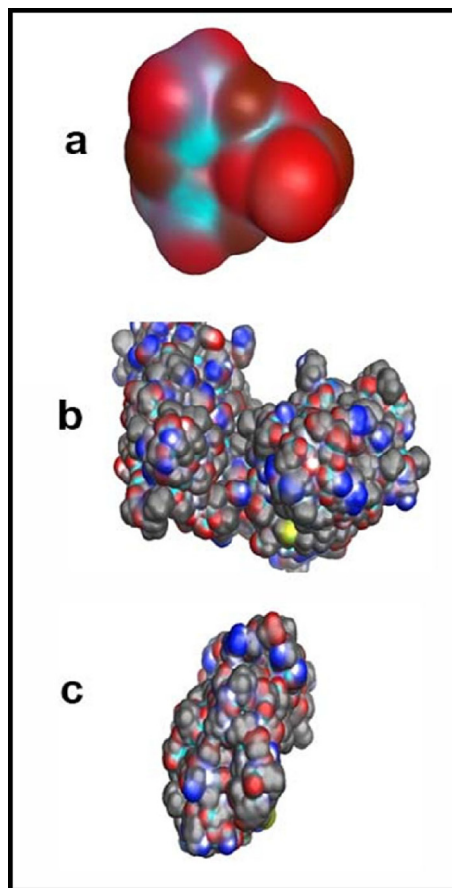


Fig. 13 Vander waals map of (a) hydroxyapatite and (b) vander waals Surface of T98 (c) vander waals Surface of SH-S5YS.

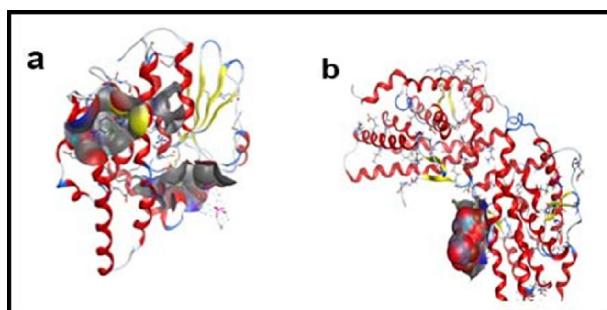


Fig. 14 (a) Vander waals surface of Hydroxyapatite- SH-S5YS complex and (b) van der waals surface of Hydroxyapatite- T98 complex.

hydroxyapatite- T98 complex respectively. According to these figures, hydroxyapatite has a more negative surface that can interact with T98 and SH-S5YS receptor molecules.

4. Conclusion

As shown in the present study, lemon extract can be used as a capping and reducing agent in the production of hydroxyapatite nanoparticles. The XRD results revealed pure particles with a size of 37 ± 2 nm which was confirmed through TEM analysis. MTT assays were used to determine the toxicity of the NPs against T98 and SH-SY5Y cancer cell lines. Both the human primary glioblastoma and neuroblastoma cancer cell lines under study were shown to be susceptible to NPs' abilities to cause cell death. A higher level of toxicity was observed in glioblastoma cells than in neuroblastoma cells for all NPs. A molecular docking calculation was conducted for the Hydroxyapatite-SH-S5YS complex and the Hydroxyapatite-T98 complex to determine their binding energies. In vivo assessments, pharmacodynamics, and pharmacokinetics studies will be necessary to better understand surface alterations.

CRedit authorship contribution statement

Mahin Baladi: Software, Investigation, Methodology, Writing – review & editing, Writing – original draft, Formal analysis. **Mahnaz Amiri:** Project administration, Formal analysis, Data curation, Investigation, Writing – review & editing, Writing – original draft. **Parisa Mohammadi:** Investigation, Formal analysis. **Karrar Salih Mahdi:** Validation, Writing – review & editing. **Zahra Golshani:** Investigation, Formal analysis. **Razieh Razavi:** Software, Formal analysis. **Masoud Salavati-Niasari:** Formal analysis, Methodology, Writing – review & editing, Writing – original draft, Conceptualization, Supervision, Project administration, Investigation, Data curation, Validation, Resources, Visualization, Funding acquisition.

Declaration of Competing Interest

The authors declare that they have no known competing financial interests or personal relationships that could have appeared to influence the work reported in this paper.

Acknowledgment

Authors are grateful to the council of Iran National Science Foundation (INSF, 97017837), and the University of Kashan for supporting this work; Grant No. (159271/MB4).

References

- Altunbek, M., Keleştemur, S., Baran, G., Çulha, M., 2018. Role of modification route for zinc oxide nanoparticles on protein structure and their effects on glioblastoma cells. *Int. J. Biol. Macromol.* 118, 271–278.
- Amiri, M., Pardakhti, A., Ahmadi-Zeidabadi, M., Akbari, A., Salavati-Niasari, M., 2018. Magnetic nickel ferrite nanoparticles: Green synthesis by *Urtica* and therapeutic effect of frequency magnetic field on creating cytotoxic response in neural cell lines. *Colloids Surf. B Biointerfaces* 172, 244–253.
- Arbo, M., Silva, R., Barbosa, D., da Silva, D.D., Silva, S., Teixeira, J. P., Bastos, M., Carmo, H., 2016. In vitro neurotoxicity evaluation of piperazine designer drugs in differentiated human neuroblastoma SH-SY5Y cells. *J. Appl. Toxicol.* 36 (1), 121–130.
- Azijli, K., Weyhenmeyer, B., Peters, G., De Jong, S., Kruyt, F., 2013. Non-canonical kinase signaling by the death ligand TRAIL in cancer cells: discord in the death receptor family. *Cell Death Differ.* 20 (7), 858–868.
- Bakan, F., Laçın, O., Sarac, H., 2013. A novel low temperature sol-gel synthesis process for thermally stable nano crystalline hydroxyapatite. *Powder Technol.* 233, 295–302.
- Bellail, A.C., Hunter, S.B., Brat, D.J., Tan, C., Van Meir, E.G., 2004. Microregional extracellular matrix heterogeneity in brain modulates glioma cell invasion. *Int. J. Biochem. Cell Biol.* 36 (6), 1046–1069.
- Catauro, M., Bollino, F., Tranquillo, E., Tuffi, R., Dell'Era, A., Cipriotti, S.V., 2019. Morphological and thermal characterization of zirconia/hydroxyapatite composites prepared via sol-gel for biomedical applications. *Ceram. Int.* 45 (2), 2835–2845.
- Chan, W.C., Khademhosseini, A., Parak, W., Weiss, P.S., 2017. Cancer: Nanoscience and nanotechnology approaches. *ACS Publications*, 4375–4376.
- Chen, W., Zheng, R., Zeng, H., Zhang, S., He, J., 2015. Annual report on status of cancer in China, 2011. *Chin. J. Cancer Res.* 27 (1), 2.
- Chu, S.-H., Feng, D.-F., Ma, Y.-B., Li, Z.-Q., 2012. Hydroxyapatite nanoparticles inhibit the growth of human glioma cells in vitro and in vivo. *Int. J. Nanomed.* 7, 3659.
- Claes, A., Idema, A.J., Wesseling, P., 2007. Diffuse glioma growth: a guerilla war. *Acta Neuropathol.* 114 (5), 443–458.
- De Wild, M., Berner, S., Suzuki, H., Ramoino, L., Baratoff, A., Junga, T.A., 2003. Molecular assembly and self-assembly a: molecular nanoscience for future technologies. *Ann. N. Y. Acad. Sci.* 1006 (1), 291–305.
- Ellor, S.V., Pagano-Young, T.A., Avgeropoulos, N.G., 2014. Glioblastoma: background, standard treatment paradigms, and supportive care considerations. *SAGE Publications Sage CA, Los Angeles, CA*.
- Geuli, O., Metoki, N., Zada, T., Reches, M., Eliaz, N., Mandler, D., 2017. Synthesis, coating, and drug-release of hydroxyapatite nanoparticles loaded with antibiotics. *J. Mater. Chem. B* 5 (38), 7819–7830.
- Ghate, P., Prabhu, D., Murugesan, G., Goveas, L.C., Varadavenkatesan, T., Vinayagam, R., Chi, N.T.L., Pugazhendhi, A., Selvaraj, R., 2022. Synthesis of hydroxyapatite nanoparticles using *Acacia falcata* leaf extract and study of their anti-cancerous activity against cancerous mammalian cell lines. *Environ. Res.* 214, 113917.
- Goudarzi, M., Alshamsi, H.A., Amiri, M., Salavati-Niasari, M., 2021. ZnCo2O4/ZnO nanocomposite: Facile one-step green solid-state thermal decomposition synthesis using *Dactylopius Coccus* as capping agent, characterization and its 4T1 cells cytotoxicity investigation and anticancer activity. *Arab. J. Chem.* 14, (9) 103316.
- Huang, C., Chen, L., Savage, S.R., Egeuz, R.V., Dou, Y., Li, Y., da Veiga Leprevost, F., Jaehrig, E.J., Lei, J.T., Wen, B., 2021. Proteogenomic insights into the biology and treatment of HPV-

- negative head and neck squamous cell carcinoma. *Cancer Cell* 39 (3), 361–379. e16.
- Kovalevich, J., Langford, D., 2013. Considerations for the use of SH-SY5Y neuroblastoma cells in neurobiology. Springer, *Neuronal Cell Culture*, pp. 9–21.
- Kundu, B., Ghosh, D., Sinha, M.K., Sen, P.S., Balla, V.K., Das, N., Basu, D., 2013. Doxorubicin-intercalated nano-hydroxyapatite drug-delivery system for liver cancer: an animal model. *Ceram. Int.* 39 (8), 9557–9566.
- Laonapakul, T., 2015. Synthesis of hydroxyapatite from biogenic wastes. *Eng. Appl. Sci. Res.* 42 (3), 269–275.
- Liu, C., Nie, W., Bao, Q., Liu, Q., Wei, C., Hua, Y., 2018. The effects of the pressure outlet's position on the diffusion and pollution of dust in tunnel using a shield tunneling machine. *Energ. Build.* 176, 232–245.
- Louis, D.N., Perry, A., Reifenberger, G., Von Deimling, A., Figarella-Branger, D., Cavenee, W.K., Ohgaki, H., Wiestler, O.D., Kleihues, P., Ellison, D.W., 2016. The 2016 World Health Organization classification of tumors of the central nervous system: a summary. *Acta Neuropathol.* 131 (6), 803–820.
- Mateus, J.C.B., 2015. Optimization of a multielectrode array (MEA)-based approach to study the impact of A β on the SH-SY5Y cell line. Universidade de Aveiro.
- Messaoudi, K., Clavreul, A., Lagarce, F., 2015. Toward an effective strategy in glioblastoma treatment. Part I: resistance mechanisms and strategies to overcome resistance of glioblastoma to temozolomide. *Drug Discovery Today* 20 (7), 899–905.
- Miller, K.D., Siegel, R.L., Lin, C.C., Mariotto, A.B., Kramer, J.L., Rowland, J.H., Stein, K.D., Alteri, R., Jemal, A., 2016. Cancer treatment and survivorship statistics, 2016. *CA: a cancer J. Clin* 66 (4), 271–289.
- Milovac, D., Ferrer, G.G., Ivankovic, M., Ivankovic, H., 2014. PCL-coated hydroxyapatite scaffold derived from cuttlefish bone: Morphology, mechanical properties and bioactivity. *Mater. Sci. Eng. C* 34, 437–445.
- Mondal, S., Pal, U., 2019. 3D hydroxyapatite scaffold for bone regeneration and local drug delivery applications. *J. Drug Delivery Sci. Technol.* 53, 101131.
- Navaneethan, M., Nithiananth, S., Abinaya, R., Harish, S., Archana, J., Sudha, L., Ponnusamy, S., Muthamizhchelvan, C., Ikeda, H., Hayakawa, Y., 2017. Hydrothermal growth of highly monodispersed TiO₂ nanoparticles: functional properties and dye-sensitized solar cell performance. *Appl. Surf. Sci.* 418, 186–193.
- Nosrati, H., Sarraf-Mamoory, R., Ahmadi, A.H., Quang Svend Le, D., Canillas Perez, M., Bunger, C.E., 2020. Effect of hydrogen gas pressure on the mechanical properties of reduced graphene oxide-HA nanocomposites. *J. Tissues Mater.* 3 (1), 21–30.
- Nosrati, H., Mamoory, R.S., Le, D.Q.S., Bünger, C.E., Emameh, R. Z., Dabir, F., 2020. Gas injection approach for synthesis of hydroxyapatite nanorods via hydrothermal method. *Mater Charact* 159, 110071.
- Parvathy, S., Manjula, G., Balachandar, R., Subbaiya, R., 2022. Green synthesis and characterization of cerium oxide nanoparticles from *Artabotrys hexapetalus* leaf extract and its antibacterial and anticancer properties. *Mater. Lett.* 314, 131811.
- Qi, L., Bellail, A.C., Rossi, M.R., Zhang, Z., Pang, H., Hunter, S., Cohen, C., Moreno, C.S., Olson, J.J., Li, S., 2011. Heterogeneity of primary glioblastoma cells in the expression of caspase-8 and the response to TRAIL-induced apoptosis. *Apoptosis* 16 (11), 1150–1164.
- Salavati-Niasari, M., 2006. Host (nanocavity of zeolite-Y)-guest (tetraaza[14]annulene copper(II) complexes) nanocomposite materials: Synthesis, characterization and liquid phase oxidation of benzyl alcohol. *J. Mol. Catal. A Chem.* 245 (1–2), 192–199. <https://doi.org/10.1016/j.molcata.2005.09.046>.
- Salavati-Niasari, M., Dadkhah, M., Davar, F., 2009. Synthesis and characterization of pure cubic zirconium oxide nanocrystals by decomposition of bis-aqua, tris-acetylacetonato zirconium (IV) nitrate as new precursor complex. *Inorg. Chim. Acta* 362 (11), 3969–3974. <https://doi.org/10.1016/j.ica.2009.05.036>.
- Sang, R., Chen, M., Yang, Y., Li, Y., Shi, J., Deng, Y., Chen, X., Yang, W., 2019. HAp@ GO drug delivery vehicle with dual-stimuli-triggered drug release property and efficient synergistic therapy function against cancer. *J. Biomed. Mater. Res. A* 107 (10), 2296–2309.
- Sladowski, D., Steer, S.J., Clothier, R.H., Balls, M., 1993. An improved MIT assay. *J. Immunol. Methods* 157 (1–2), 203–207.
- Sodhani, H., Hedaoo, S., Murugesan, G., Pai, S., Vinayagam, R., Varadavenkatesan, T., Bharath, G., Hajja, M.A., Nadda, A.K., Govarathanan, M., 2022. Adsorptive removal of Acid Blue 113 using hydroxyapatite nanoadsorbents synthesized using *Peltophorum pterocarpum* pod extract. *Chemosphere* 299, 134752.
- Subbaiya, R., Saravanan, M., Priya, A.R., Shankar, K.R., Selvam, M., Ovais, M., Balajee, R., Barabadi, H., 2017. Biomimetic synthesis of silver nanoparticles from *Streptomyces atrovirens* and their potential anticancer activity against human breast cancer cells. *IET Nanobiotechnol.* 11 (8), 965–972.
- Sun, J., Ding, T., 2009. p53 reaction to apoptosis induced by hydroxyapatite nanoparticles in rat macrophages. *J. Biomedical Mater. Res. Part A: An Official J. Soc. Biomater. The Japanese Soc. Biomater. Aust. Soc. Biomater. Korean Soc. Biomater.* 88 (3), 673–679.
- Szczęs, A., Hołysz, L., Chibowski, E., 2017. Synthesis of hydroxyapatite for biomedical applications. *Adv. Colloid Interface Sci.* 249, 321–330.
- Tang, W., Yuan, Y., Liu, C., Wu, Y., Lu, X., Qian, J., 2014. Differential cytotoxicity and particle action of hydroxyapatite nanoparticles in human cancer cells. *Nanomedicine* 9 (3), 397–412.
- Tao, F., Ma, S., Tao, H., Jin, L., Luo, Y., Zheng, J., Xiang, W., Deng, H., 2021. Chitosan-based drug delivery systems: from synthesis strategy to osteomyelitis treatment—a review. *Carbohydr. Polym.* 251, 117063.
- Torre, L.A., Bray, F., Siegel, R.L., Ferlay, J., Lortet-Tieulent, J., Jemal, A., 2012. Global cancer statistics, 2012. *CA: a cancer J. Clin.* 65 (2), 87–108.
- Venkatesan, J., Pallela, R., Bhatnagar, I., Kim, S.-K., 2012. Chitosan-amylopectin/hydroxyapatite and chitosan-chondroitin sulphate/hydroxyapatite composite scaffolds for bone tissue engineering. *Int. J. Biol. Macromol.* 51 (5), 1033–1042.
- Vinayagam, R., Pai, S., Murugesan, G., Varadavenkatesan, T., Kaviyarasu, K., Selvaraj, R., 2022. Green synthesized hydroxyapatite nanoadsorbent for the adsorptive removal of AB113 dye for environmental applications. *Environ. Res.* 212, 113274.
- Wahl, D., Czernuszka, J., 2006. Collagen-hydroxyapatite composites for hard tissue repair. *Eur Cell Mater* 11 (1), 43–56.
- Wang, S., 2008. The promise of cancer therapeutics targeting the TNF-related apoptosis-inducing ligand and TRAIL receptor pathway. *Oncogene* 27 (48), 6207–6215.
- Xiong, H., Du, S., Ni, J., Zhou, J., Yao, J., 2016. Mitochondria and nuclei dual-targeted heterogeneous hydroxyapatite nanoparticles for enhancing therapeutic efficacy of doxorubicin. *Biomaterials* 94, 70–83.
- Xu, R., Zhang, G., Mai, J., Deng, X., Segura-Ibarra, V., Wu, S., Shen, J., Liu, H., Hu, Z., Chen, L., 2016. An injectable nanoparticle generator enhances delivery of cancer therapeutics. *Nat. Biotechnol.* 34 (4), 414–418.
- Yuan, X., Gajan, A., Chu, Q., Xiong, H., Wu, K., Wu, G.S., 2018. Developing TRAIL/TRAIL death receptor-based cancer therapies. *Cancer Metastasis Rev.* 37 (4), 733–748.
- Zhao, Y., Tian, B., Wang, Y., Ding, H., 2017. Kaempferol sensitizes human ovarian cancer cells-OVCAR-3 and SKOV-3 to tumor necrosis factor-related apoptosis-inducing ligand (TRAIL)-induced apoptosis via JNK/ERK-CHOP pathway and up-regulation of death receptors 4 and 5. *Medical science monitor: Int. Med. J. Experimental Clin. Res.* 23, 5096.

Zhou, Z.-C., Lin, Z.-J., Shuai, X.-Y., Zheng, J., Meng, L.-X., Zhu, L., Sun, Y.-J., Shang, W.-C., Chen, H., 2021. Temporal variation and sharing of antibiotic resistance genes between water and wild fish gut in a peri-urban river. *J. Environ. Sci.* 103, 12–19.

Zhou, Z.-F., Sun, T.-W., Qin, Y.-H., Zhu, Y.-J., Jiang, Y.-Y., Zhang, Y., Liu, J.-J., Wu, J., He, S.-S., Chen, F., 2019. Selenium-doped hydroxyapatite biopapers with an anti-bone tumor effect by inducing apoptosis. *Biomater. Sci.* 7 (12), 5044–5053.